Interaction between Faraday rotation and Cotton–Mouton effects in polarimetry modeling for NSTX[a)]

J. Zhang,[b)] N. A. Crocker, T. A. Carter, S. Kubota, and W. A. Peebles
Department of Physics and Astronomy, UCLA, Los Angeles, California 90095-1547, USA

(Presented 17 May 2010; received 14 May 2010; accepted 7 July 2010; published online 6 October 2010)

The evolution of electromagnetic wave polarization is modeled for propagation in the major radial direction in the National Spherical Torus Experiment with retroreflection from the center stack of the vacuum vessel. This modeling illustrates that the Cotton–Mouton effect–ellipticization due to the magnetic field perpendicular to the propagation direction–is shown to be strongly weighted to the high-field region of the plasma. An interaction between the Faraday rotation and Cotton–Mouton effects is also clearly identified. Elliptization occurs when the wave polarization direction is neither parallel nor perpendicular to the local transverse magnetic field. Since Faraday rotation modifies the polarization direction during propagation, it must also affect the resultant elliptization. The Cotton–Mouton effect also intrinsically results in rotation of the polarization direction, but this effect is less significant in the plasma conditions modeled. The interaction increases at longer wavelength and complicates interpretation of polarimetry measurements. © *2010 American Institute of Physics.*
[doi:10.1063/1.3479042]

I. INTRODUCTION

Polarimetry is a powerful technique for probing magnetic field equilibria[1] and fluctuations,[2] plasma density,[3] and current density[4] profiles in magnetically confined plasmas. It measures changes in the electromagnetic (EM) wave polarization caused by propagation through a magnetized plasma. This diagnostic has been routinely used on conventional high aspect ratio tokamaks (e.g., JET)[5] and reversed field pinches (RFP, e.g., MST).[2] However, no detailed study of polarimetry has been performed for propagation in the major radial direction in spherical tori. In contrast with conventional tokamaks and RFP, in spherical tori both magnetic field strength and direction vary strongly in the major radial direction. This work models the evolution of EM wave polarization along major radial chords of varying heights with retroreflection in the National Spherical Torus Experiment (NSTX),[6] using Mueller–Stokes calculus. (Major radial chords are horizontal chords radiating from the center stack of vacuum vessel.) The motivation for this modeling is to help the design of a polarimeter system planned for NSTX. The Cotton–Mouton effect–elliptization due to the magnetic field perpendicular to the propagation direction–is shown to be strongly weighted to the high-field region in NSTX. An interaction between the Faraday rotation (FR) and Cotton–Mouton (CM) effects is also clearly identified. Elliptization occurs when the wave polarization direction is neither parallel nor perpendicular to the local transverse magnetic field. Since FR modifies the polarization direction during propagation, it must also affect the resultant elliptization. The CM effect also intrinsically results in rotation of the polarization direction, but this effect is less significant in the plasma conditions modeled. The interaction is shown to increase with wavelength.

The interaction is present when the magnetic field has both parallel and perpendicular components with respect to the wave propagation direction. It complicates the interpretation of polarimetry measurements, especially at longer wavelength. Previous polarimetry studies focused separately on FR[7–9] or the CM effect.[3] Recent results combining measurement and modeling including both effects on JET also assume one effect or the other is small.[5,10]

Most of the modeling results presented here focus on 288 GHz ($\lambda = 1.04$ mm) microwaves launched with linear initial polarization in a typical neutral-beam-heated L-mode plasma in NSTX. The millimeter wavelength used is longer than common for polarimetry systems, but it is a good compromise between two competing constraints. At longer wavelength the effects of the plasma on polarization are stronger, allowing for more sensitive measurement of magnetic fluctuations. At shorter wavelength, refraction becomes less significant. In the following sections, the polarimetry model is described and results are shown for modeling using a plasma density profile from Thomson scattering measurements and a magnetic field profile from EFIT (equilibrium fitting code)[11] in NSTX.

II. POLARIMETRY MODELING DESCRIPTION

Several assumptions are made to simplify the calculation of polarization evolution. A cold plasma model is adopted, which excludes corrections from finite temperature effects.[12] The plasma is assumed to be collisionless, so the beam experiences no dissipation. The Wentzel-Kramers-Brillouin

[a)]Contributed paper, published as part of the Proceedings of the 18th Topical Conference on High Temperature Plasma Diagnostics, Wildwood, New Jersey, May 2010.
[b)]Electronic mail: xyzhangj@physics.ucla.edu.

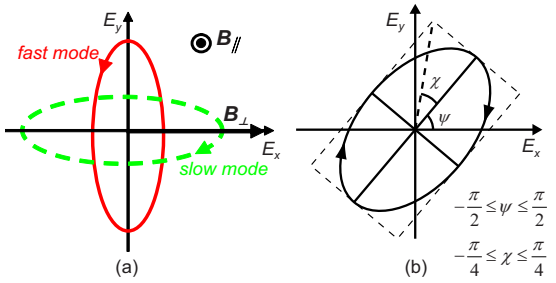

FIG. 1. (Color online) (a) Fast (solid line) and slow (dashed line) characteristic modes. The fast mode has a major axis perpendicular to $\vec{B}_\perp$ and right-handedness with respect to $\vec{B}_\parallel$. $\perp$ and $\parallel$ are defined with respect to the propagation direction. (b) Polarization properties are characterized by χ (*ellipticization angle*, where right/left handedness are represented by +/− sign) and ψ (*polarization direction angle*); their ranges are also shown.

approximation[13] is used, i.e., plasma parameters are assumed to be slowly varying $(|\vec{B}| \gg |(1/k)(\partial \vec{B}/\partial z)|, n \gg |(1/k) \times (\partial n/\partial z)|)$. Also cutoffs and resonances are not considered. Only the electron response is included; the contribution from ion motion is ignored $(\omega_{pi}, \omega_{ci} \ll \omega_{pe}, \omega_{ce} \ll \omega$, where ω is the angular frequency of the probing beam, $\omega_p = \sqrt{nq^2/m\varepsilon_0}$, $\omega_c = |q|B/m$, and subscripts i and e stand for ions and electrons, respectively). Refraction is also neglected, so it is assumed that the beam path through the plasma is straight and that the beam neither diverges nor converges.

The polarization of an EM wave changes as it propagates through a magnetized plasma due to plasma birefringence and optical activity. The plasma features a pair of fast and slow characteristic modes (i.e., EM waves that propagate with their polarizations unchanged) whose phase velocities and polarizations are determined by local plasma parameters at any position along the wave path [Fig. 1(a)]. The two modes are generally elliptically polarized with orthogonal polarization directions and opposite handedness. The fast mode has a major axis perpendicular to $\vec{B}_\perp$ and right-handedness with respect to $\vec{B}_\parallel$. ($\perp$ and $\parallel$ are defined with respect to the propagation direction.) An EM wave of any polarization may be represented as some combination of this pair of characteristic modes. The combined polarization is sensitive to the relative phase of its two components, so a difference in their phase velocities causes the polarization to change. The FR and CM effects are two well-known special cases. In FR, where the wave propagates parallel to a magnetic field, the characteristic modes are circularly polarized. For the CM effect, where the wave propagates perpendicular to a magnetic field, the fast and slow modes, which are linearly polarized, are the extraordinary and ordinary modes, respectively.

The modeling presented here uses the Mueller–Stokes calculus.[14] The ellipse representing the polarization of a single-frequency EM wave is characterized by two parameters, *elliptization angle* χ and *polarization direction angle* ψ [Fig. 1(b)]. The polarization state of the wave can be mapped by the *Stokes vector* $\vec{s}$ [Eq. (1)] to a point on a unit sphere in an abstract space referred to as the *Poincaré sphere*. For instance, alignment of $\vec{s}$ with the s_3 axis corresponds to circular polarization, while a vanishing s_3 component corresponds to linear polarization in the laboratory frame. As a wave propagates through a magnetized plasma, its polarization changes and the corresponding Stokes vector traces out a trajectory on the Poincaré sphere. Each small step of the trajectory results from a small rotation of the Stokes vector around an axis given by the vector $\vec{\Omega}$ which is determined everywhere along the wave path by local plasma parameters [Eq. (2)]. The z coordinate indicates position along the wave path and c is speed of light in vacuum.

$$\begin{pmatrix} s_1 \\ s_2 \\ s_3 \end{pmatrix} = \begin{pmatrix} \cos 2\chi \cos 2\psi \\ \cos 2\chi \sin 2\psi \\ \sin 2\chi \end{pmatrix}, \tag{1}$$

$$\frac{d\vec{s}(z)}{dz} = \vec{\Omega}(z) \times \vec{s}(z),$$

$$\vec{\Omega} = \frac{\omega_{pe}^2 \omega_{ce}^2}{2c\omega(\omega^2 - \omega_{ce}^2)} \begin{bmatrix} (B_x^2 - B_y^2)/B^2 \\ 2B_x B_y/B^2 \\ 2(\omega/\omega_{ce})B_z/B \end{bmatrix}. \tag{2}$$

The origin of the interaction between the FR and CM effects can be seen clearly from the preceding geometrical description of the polarization evolution. Both the FR and CM effects are directly related to the components of $\vec{\Omega}$. A nonvanishing Ω_3 gives rise to FR by causing a rotation of $\vec{s}$ about the s_3 axis. This corresponds to a rotation of the wave polarization ellipse in the laboratory frame. A nonvanishing Ω_1 or Ω_2 gives rise to the CM effect by causing a change in s_3 and therefore in the ellipticity of the wave polarization ellipse. However, the way in which s_3 changes clearly depends on the direction of $\vec{s}$ relative to $\vec{\Omega}$, which can be influenced by FR.

The interaction may also be seen from the differential expressions relating changes in χ and ψ to the FR and CM effects[15]

$$d\chi = \tfrac{1}{2} \sin 2\psi d\delta|_{CM}, \tag{3}$$

$$d\psi = d\psi|_{FR} - \tfrac{1}{2} \tan 2\chi \cos 2\psi d\delta|_{CM}, \tag{4}$$

$$d\psi|_{FR} = -\frac{\omega_{pe}^2 \omega_{ce}}{2c\omega^2} \frac{B_\parallel}{B} dz, \tag{5}$$

$$d\delta|_{CM} = \frac{\omega_{pe}^2 \omega_{ce}^2}{2c\omega^3} \left(\frac{B_\perp}{B}\right)^2 dz, \tag{6}$$

where δ is the relative phase between the x and y components of the wave electric field. Equations (3) and (4) assume the coordinate system illustrated in Fig. 1(b) where the x axis is aligned with $\vec{B}_\perp$. Equation (3) shows the sensitivity of elliptization to ψ. FR modifies ψ, so it affects elliptization. The second term on the right hand side of Eq. (4) shows that the CM effect also intrinsically causes polarization rotation. For the modeling performed in this paper, where the radial views studied are well above the plasma midplane (i.e., ≥ 0.1 m), this contribution to the total polarization rotation is small ($<15\%$). This is because throughout the majority of the wave path, either the absolute elliptization angle is small (i.e., $|\chi| \ll 45°$) or the CM effect is much weaker than the FR

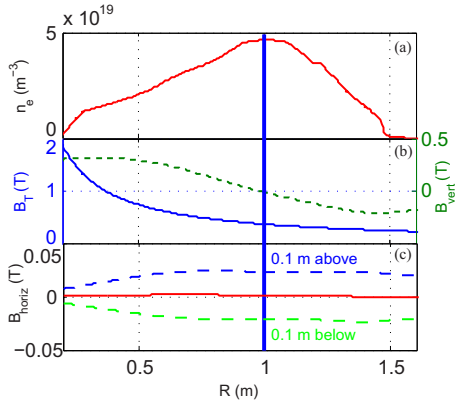

FIG. 2. (Color online) (a) Density profile of a typical neutral-beam-heated L-mode plasma for modeling. (shot no. 124764, 0.325 s). (b) Toroidal (solid line) and vertical (dashed line) magnetic fields along major radius in the midplane (they vary little with height near the midplane). (c) Horizontal (i.e., radial) magnetic field along major radius 0.1 m above, below (dashed lines), and in the midplane (solid line).

(i.e., $|d\delta|_{CM} \ll |d\psi|_{FR}$). The following discussion will focus on the impact of FR on elliptization. It should be noted that along the chords close to the midplane where FR is weak the rotation caused by the CM effect can be dominant.

III. MODELING RESULTS AND DISCUSSION

The modeling results discussed here are obtained in a typical neutral-beam-heated L-mode plasma (shot no. 124764, 0.325 s) (Fig. 2), which has a major radius of $R_0 = 0.85$ m and a minor radius $a = 0.67$ m. The density profile is centrally peaked with a maximum of $n_0 = 4.7 \times 10^{19}$ m^{-3} at $R_{axis} = 1.0$ m. The electron plasma and cyclotron frequencies are $f_{pe} = 61.4$ GHz and $f_{ce} = 10.5$ GHz on axis.

The modeling shows that the magnitude of the elliptization angle increases most rapidly when the wave is in the high-field region ($R < R_{axis}$) (Fig. 3). This stands in contrast with conventional tokamaks. Elliptization is sensitive to the strength of the perpendicular magnetic field [Eq. (3)], of which the toroidal magnetic field B_T is a significant component. B_T varies approximately inversely with major radius in both conventional tokamaks and spherical tori, but in spherical tori, the variation is much stronger because of their relatively low aspect ratio. For instance, in NSTX ($R_0/a \simeq 1.27$) B_T varies from 0.2 T at the outer edge ($R = 1.6$ m) to 2 T close to the center stack ($R = 0.2$ m) [Fig. 2(c)].

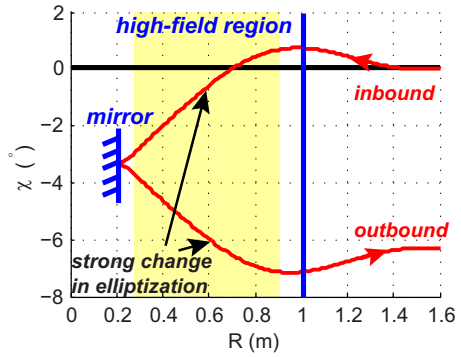

FIG. 3. (Color online) Evolution of elliptization angle (χ) along chord in midplane for waves with horizontal linear polarization at launch (i.e., in toroidal direction). Vertical solid line indicates plasma center (i.e., peak density). The mirror is mounted on the center stack. ($f = 288$ GHz, $\lambda = 1.04$ mm).

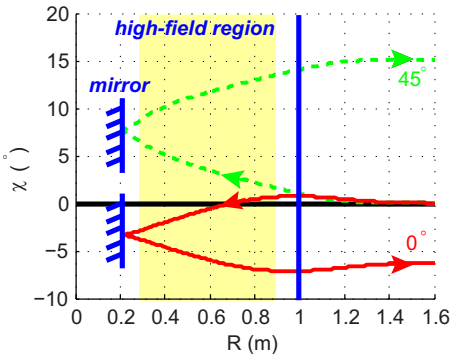

FIG. 4. (Color online) Evolution of elliptization angle (χ) along chord in midplane for waves with horizontal (solid line) and 45° (dashed line) linear polarizations at launch. Zero elliptization (i.e., linearly polarized) is highlighted on the grid. ($f = 288$ GHz, $\lambda = 1.04$ mm).

Modeling shows that the evolution of the elliptization depends strongly on the polarization direction in the high-field region. Figure 4 shows the dramatically different elliptization evolution for two waves launched in the midplane with launch angles of 0° and 45°. This dependence is expected since elliptization is strongly weighted to the high-field region and sensitive to ψ [Eq. (3)]. For a chord in the midplane, the polarization direction in the high-field region is determined by the launch angle since FR is very weak there ($\vec{B}_\parallel$ is weak in the midplane).

Of particular interest, the modeling shows that FR can play a significant role in elliptization. Chords away from the midplane can have significant $\vec{B}_\parallel$, so FR can substantially change the polarization direction of the wave before it enters the high-field region. Figure 5 compares the elliptization evolution of a wave launched with horizontal linear polarization both with and without the influence of FR. The final elliptization of the wave is very different for the two cases. The modeled chord is 0.1 m above the midplane, where $|\vec{B}_\parallel|$ reaches a maximum of 0.024 T along the chord. For the case without FR, $\vec{B}_\parallel$ is simply set uniformly to zero along the chord. The impact of FR on elliptization identified here is a primary element of the interaction between the two effects.

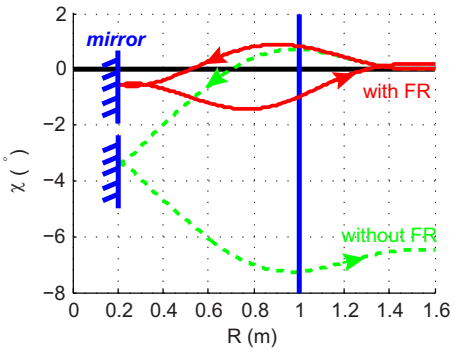

FIG. 5. (Color online) Evolution of elliptization angle (χ) for waves with horizontal linear polarization at launch along a chord 0.1 m above midplane with (solid line) and without (dashed line) FR. FR is eliminated by setting $\vec{B}_\parallel = 0$ along the chord. ($f = 288$ GHz, $\lambda = 1.04$ mm).

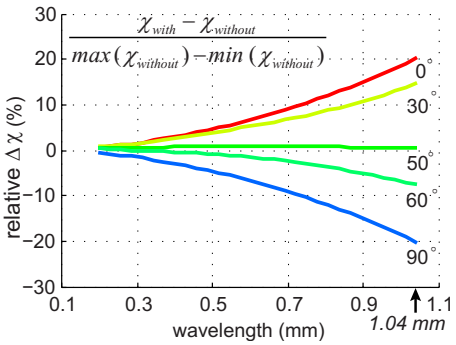

FIG. 6. (Color online) Difference between the final elliptizations with and without FR ($\Delta\chi$) vs wavelength for different launch angles. $\Delta\chi$ is normalized by the difference between the maximum and minimum final values of χ without FR.

Modeling shows a significant wavelength dependence in the strength of the impact of FR on elliptization. Both the FR and CM effects are expected to become stronger with increasing wavelength [Eqs. (5) and (6)]. However, it is not obvious whether the impact of FR on elliptization should become more or less significant as the wavelength increases. To assess this, the change in the final value of χ caused by including FR is calculated (Fig. 6). The change $\Delta\chi$ is normalized by the difference between the maximum and minimum final values of χ without FR. This normalization factor serves as a measure of the strength of the elliptization effect. Figure 6 shows that the relative effect of FR on elliptization increases with wavelength.

The interaction complicates the interpretation of polarimetry measurements if both the FR and CM effects are large. For instance, this is the case for the planned "48,57 μm poloidal polarimeter" in ITER[16] if the CM effect is large enough to be used as an alternative plasma density measurement. Under these conditions, the common practice of simply integrating either Eq. (5) or Eq. (6) to obtain the approximate total polarization rotation or elliptization,[5] respectively, is no longer valid. Also, the interpretation of an array of chord measurements used to characterize the equilibrium[1,17] becomes more complicated. The profile of rotation of polarization direction versus chord impact parameter is affected by the interaction, leading to a change in both the zero crossing and slope.

IV. CONCLUSION

The modeling presented here shows that the CM effect is strongly weighted to the high-field region of NSTX. An interaction between the FR and CM effects is clearly identified. Since FR modifies the polarization direction as the wave propagates, it must also affect the resultant elliptization. The CM effect also intrinsically results in rotation of the polarization direction, but this is less significant to the modeling results presented here. The interaction identified here is shown to increase in significance with wavelength. Care has to be taken in interpreting the polarimetry measurement if both effects are large.

ACKNOWLEDGMENTS

The authors are grateful for the contributions of the NSTX research team. This work is supported by U.S. DOE under Contract No. DE-FG02-99ER54527.

[1] D. L. Brower, W. X. Ding, S. D. Terry, J. K. Anderson, T. M. Biewer, B. E. Chapman, D. Craig, C. B. Forest, S. C. Prager, and J. S. Sarff, Phys. Rev. Lett. **88**, 185005 (2002).
[2] W. X. Ding, D. L. Brower, S. D. Terry, D. Craig, S. C. Prager, J. S. Sarff, and J. C. Wright, Phys. Rev. Lett. **90**, 035002 (2003).
[3] Ch. Fuchs and H. J. Hartfuss, Phys. Rev. Lett. **81**, 1626 (1998).
[4] H. Soltwisch, Plasma Phys. Controlled Fusion **34**, 1669 (1992).
[5] A. Boboc, L. Zabeo, A. Murari, and JET-EFDA Contributors, Rev. Sci. Instrum. **77**, 10F324 (2006).
[6] M. Ono, S. M. Kaye, Y.-K. M. Peng, G. Barnes, W. Blanchard, M. D. Carter, J. Chrzanowski, L. Dudek, R. Ewig, D. Gates, R. E. Hatcher, T. Jarboe, S. C. Jardin, D. Johnson, R. Kaita, M. Kalish, C. E. Kessel, H. W. Kugel, R. Maingi, R. Majeski, J. Manickam, B. McCormack, J. Menard, D. Mueller, B. A. Nelson, B. E. Nelson, C. Neumeyer, G. Oliaro, F. Paoletti, R. Parsells, E. Perry, N. Pomphrey, S. Ramakrishnan, R. Raman, G. Rewoldt, J. Robinson, A. L. Roquemore, P. Ryan, S. Sabbagh, D. Swain, E. J. Synakowski, M. Viola, M. Williams, J. R. Wilson, and NSTX Team, Nucl. Fusion **40**, 557 (2000).
[7] H. Soltwisch, Rev. Sci. Instrum. **57**, 1939 (1986).
[8] E. Zilli, M. O'Gorman, L. Giudicotti, F. Milani, S. L. Prunty, A. Murari, and A. Boboc, Int. J. Infrared Millim. Waves **21**, 1673 (2000).
[9] M. A. V. Zeeland, R. L. Boivin, T. N. Carlstrom, and T. M. Deterly, Rev. Sci. Instrum. **21**, 10E719-3 (2008).
[10] F. P. Orsitto, A. Boboc, C. Mazzotta, E. Giovannozzi, L. Zabeo, and JET-EFTA Contributors, Plasma Phys. Controlled Fusion **50**, 115009 (2008).
[11] L. Lao, H. John, R. Stambaugh, A. Kellman, and W. Pfeiffer, Nucl. Fusion **25**, 1611 (1985).
[12] V. V. Mirnov, W. X. Ding, D. L. Brower, M. A. V. Zeeland, and T. N. Carlstrom, Phys. Plasmas **14**, 102105 (2007).
[13] D. G. Swanson, *Plasma Waves* (CRC, Boca Raton, 2003).
[14] S. E. Segre, Plasma Phys. Controlled Fusion **41**, R57 (1999).
[15] K. Guenther and JET-EFDA Contributors, Plasma Phys. Controlled Fusion **46**, 1423 (2004).
[16] R. Pavlichenko, K. Kawahata, and T. Donne, J. Plasma Fusion Res. **2**, S1040 (2007).
[17] J. H. Rommers and J. Howard, Plasma Phys. Controlled Fusion **38**, 1805 (1996).